ACS APPLIED MATERIALS & INTERFACES

Research Article

www.acsami.org

Increasing Photocurrents in Dye Sensitized Solar Cells with Tantalum-Doped Titanium Oxide Photoanodes Obtained by Laser Ablation

Rudresh Ghosh,[†] Yukihiro Hara,[†] Leila Alibabaei,[†,‡] Kenneth Hanson,[‡] Sylvie Rangan,[§] Robert Bartynski,[§] Thomas J. Meyer,[‡] and Rene Lopez*[,†]

[†]Department of Physics and Astronomy, University of North Carolina, Chapel Hill, North Carolina, United States

[‡]Department of Chemistry, University of North Carolina, Chapel Hill, North Carolina, United States

[§]Department of Physics, Rutgers University, New Jersey, United States

Supporting Information

ABSTRACT: Laser ablation is employed to produce vertically aligned nanostructured films of undoped and tantalum-doped TiO_2 nanoparticles. Dye-sensitized solar cells using the two different materials are compared. Tantalum-doped TiO_2 photoanode show 65% increase in photocurrents and around 39% improvement in overall cell efficiency compared to undoped TiO_2. Electrochemical impedance spectroscopy, Mott–Schottky analysis and open circuit voltage decay is used to investigate the cause of this improved performance. The enhanced performance is attributed to a combination of increased electron concentration in the semiconductor and a reduced electron recombination rate.

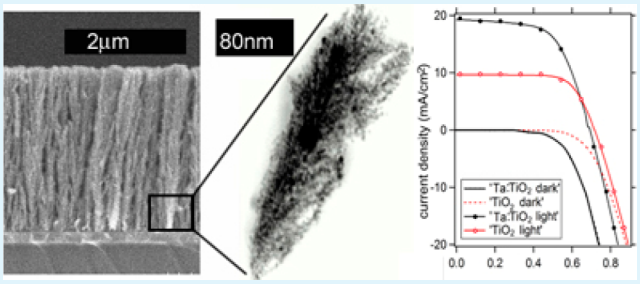

KEYWORDS: *dye sensitized solar cells, pulsed laser deposition, tantalum-doped titanium oxide, emerging photovoltaics, photocurrent, electrochemical impedance spectroscopy*

INTRODUCTION

To increase the commercial viability of solar energy conversion technology there is a need for high efficiency systems with low fabrication and material costs. Dye-sensitized solar cells (DSSC), first introduced by O'Regan and Gratzel,[1] have the potential to satisfy these requirements. In a typical DSSC, a highly porous network of TiO_2 nanoparticles provides a high surface area structure for dye adsorption and an interconnected pathway for transport of photoinjected electrons. However, losses due to inefficient excited-state electron injection from the dye into the conduction band of TiO_2 and current losses during the transport of injected electrons through the TiO_2 are inhibitory to high overall cell efficiencies.[2]

One strategy to improve cell efficiency is to enhance the electron transport, by using crystalline TiO_2 nanowires with better diffusion lengths[3−7] or hierarchical meso-structures,[8−11] which might shorten the carrier's paths. Recently pulsed laser deposition (PLD) has been used separately by others[12,13] and ourselves[14] to merge components of each of these structures with an architecture that was aptly named a "nanoforest".

An alternative strategy to improve device performance relies on changing TiO_2 transport properties by metal ion doping. This strategy has been used earlier to improve V_{oc}, J_{sc}, and fill factors in DSSCs.[15,16] For example, increases in either V_{oc}[18] or J_{sc}[19] has been observed upon doping TiO_2 with tantalum. However, the contradictory results of refs 18 and 19 may be due to the different fabrication processes used for obtaining undoped and doped materials. It is therefore important to be able to fabricate both oxides under exactly the same conditions to be able to ascertain the effect of doping alone.

In this work, we combine the best aspects of these two strategies to create hierarchical mesostructures of TiO_2 doped with tantalum ($Ta:TiO_2$) in an effort to improve overall device efficiency of DSSCs with N719 dye (ditetrabutylammonium cis-bis(isothiocyanato)bis(2,2′-bipyridyl-4,4′-dicarboxylato)-ruthenium(II)), as the chromophore.

EXPERIMENTAL SECTION

TiO_2 and $Ta:TiO_2$ nanoforest films were coated on fluorine-doped Tin oxide (FTO) glass substrates by pulsed laser deposition (PLD) from their corresponding targets (Kurt J Lesker, both 99.99% purity, 1.0 atomic % Ta in the doped one) with a KrF excimer laser (248 nm, 300 mJ, 80 Hz). The laser was focused with a 60° incidence angle into the chamber and rastered over the target (pulse fluence = 0.5 mJ/cm^2). The resulting plume was directed at the FTO glass held 5 cm above the target. Both the target and the FTO substrate were continuously rotated at 40 and 20 rpm, respectively, for uniform deposition.

Received: May 25, 2012
Accepted: August 6, 2012
Published: August 6, 2012

 © 2012 American Chemical Society

Background pressure of 100 mTorr of oxygen was maintained in the chamber during the deposition process. Prior to deposition, the PLD chamber was evacuated to a base pressure of 6×10^{-6} Torr and postdeposition annealing of the films was carried out at 450 C in air for 1 h .

Scanning electron microscope images were obtained using a Hitachi S-4700 operated at an accelerating voltage of 2 kV. Transmission electron microscope images were obtained in the normal transmission (TEM) mode and scanning (STEM) mode using JEOL 2010F-FasTEM using 200 kV accelerating voltage. Elemental mapping was done using STEM mode using INCA EnergyTEM 250 TEM microanalysis system with imaging capabilities. Chemical composition and metal oxidation states of the Ta:TiO_2 were obtained using X-ray photoelectron spectroscopy (XPS) on a Thermo K-alpha system using an Al−Kα monochromated source. X-ray diffraction investigations were done using a Rigaku MultiFlex X-ray Diffractometer, Cu Kα radiation, 40 kV−40 mA at a scan speed of 4°/min.

Both TiO_2 and Ta:TiO_2 were derivatized with N719 using the "hot slide" technique where the films were heated to 500 C for 30 min immediately prior to derivatization by the complex. The films were submerged in 0.3 mM N719 dye in acetontrile/*tert*-butanol (1:1) solution overnight. Surface dye loading was determined through UV−visible spectroscopy incorporating an integrating sphere to eliminate absorbance errors due to reflection and scattering.

Dye-sensitized sandwich cells based on the N719 derivatized photoanodes were constructed following the procedures described by Z.-S. Wang et al.,[20] with a Pt-coated FTO counter and a 25 μm Surlyn spacer. The redox electrolyte for device measurements was 0.05 M LiI, 0.03 M I_2, 1 M dimethyl propyl imidazolium iodide, 0.1 M guanidinium thiocyanate and 0.5 M *tert*-butylpyridine in dried acetonitrile: valeronitrile (85:15) (v:v). A reflective coating consisting of an aluminum foil is taped to the back end of the sandwich cell to reflect unabsorbed light back into the cell.

Flat-band potentials of the two types of samples were obtained from space charge capacitance values following Mott−Schottky analysis. To acquire the Mott−Schottky plots, electrochemical impedance spectroscopy was done over frequency ranges of 1−100 000 Hz for potentials varying from −550 to 550 mV. The devices were made in a similar fashion as mentioned in the previous section. Films used for Mott−Schottky plots were not sensitized. Electrolyte used for obtaining the Mott−Schottky plots consisted of 0.05 M I_2 and 0.5 M LiI in dried acetonitrile. It has been previously argued that capacitance data fitted from electrochemical impedance spectroscopy measurements is more reliable than single frequency measurements because the Faradaic contributions from the electrolyte cannot be neglected at negative applied potentials.[21] The model used to fit the space-charge capacitance is the same as used in ref 21.

Cell current−voltage characteristics, electrochemical impedance spectroscopy measurements, as well as Open Circuit Voltage Decay measurements were performed on sensitized samples using a Gamry500 potentiostat using Gamry Framework. An AM1.5 1 sun solar simulator (NEWPORT 1000-W Xe lamp and an AM1.5 filter) was employed as the light source for cell irradiation.

RESULTS AND DISCUSSION

The consistency, reproducibility and thickness control of films grown by laser ablation is a significant advantage of the pulsed laser deposition system compared to traditional sol gel techniques. Additionally, the similar growth rates for TiO_2 and Ta-doped TiO_2 (1.7 μm for every 100 000 shots) allow us the liberty of using exactly the same growth conditions to obtain structurally identical films. Four different film thicknesses for both Ta:TiO_2 and TiO_2 were obtained by changing the total number of laser pulses (100k, 200k, 400k, 800k shots).

As demonstrated earlier,[12,13] the metal oxide films using laser ablation under a background oxygen pressure, exhibit a forest-like vertically aligned nanostructure. Scanning and transmission electron microscopy images of the nanoforest are shown in (Figure1 a and b). The average particle size, found by analyzing TEM micrographs, is approximately 15 nm in diameter.

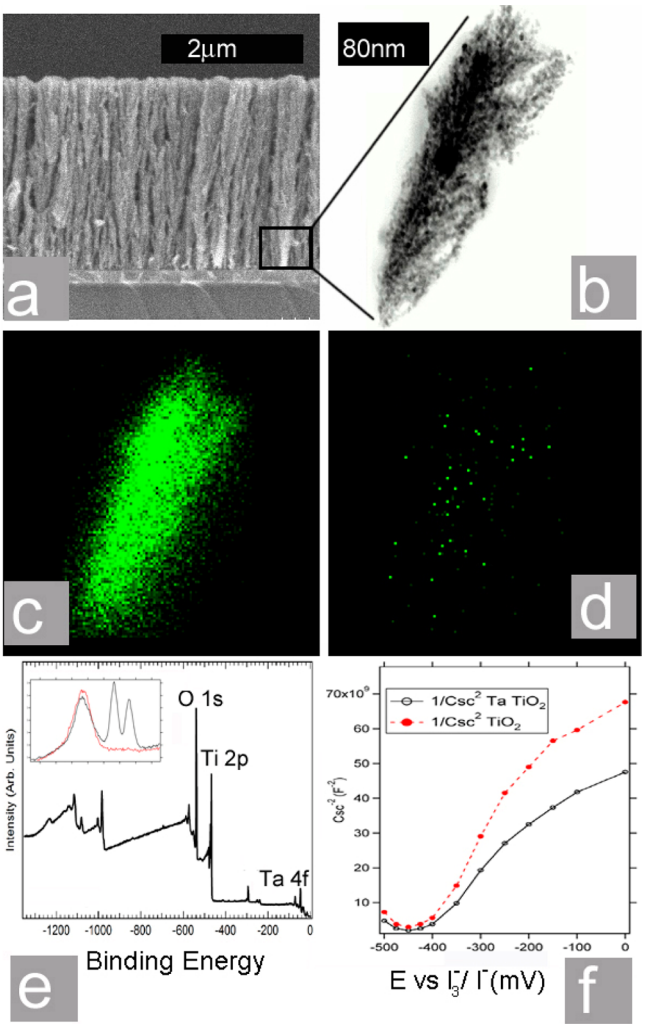

Figure 1. (a) Laser ablated Ta:TiO_2 shows vertically aligned hierarchical nanostructure, STEM image of (b) Ta:TiO_2 base of the structure, (c) elemental mapping for Ti, (d) elemental mapping for Ta, (e) X-ray photoelectron spectroscopy of Ta:TiO_2, inset shows the Ta-4f peaks clearly visible for the Ta-doped sample and not in undoped TiO_2, and (f) Mott−Schottky plot for the two nanoporous oxides on FTO contact.

Crystalinity studies using XRD show no significant difference in structure between the doped and undoped films (figure in SI).

The chemical composition and electronic structure of Ta:TiO_2 were obtained by using X-ray photoelectron spectroscopy (XPS) (Figure 1e). The presence of the Ta 4f peak confirms the presence of Ta^{5+} in the sample. Atomic concentration of Ta, from XPS analysis, of the Ta:TiO_2 film (0.9%) is in good agreement with the concentration of the PLD target (~1%). Elemental mapping, using STEM, indicate that Ta doping is uniform throughout the Ta:TiO_2 network (Figure 1c, 1d).

The current−density voltage curves for Ta:TiO_2 and TiO_2 devices for films grown from 800 000 shots (13.6 μm) can be seen in Figure 2b. The Ta:TiO_2 samples exhibit improved photocurrent (J_{sc} = 15.9 mA/cm^2) over the undoped films (J_{sc} = 9.67 mA/cm^2). The trend toward larger J_{sc} and IPCE values

dx.doi.org/10.1021/am300938g | ACS Appl. Mater. Interfaces 2012, 4, 4566−4570

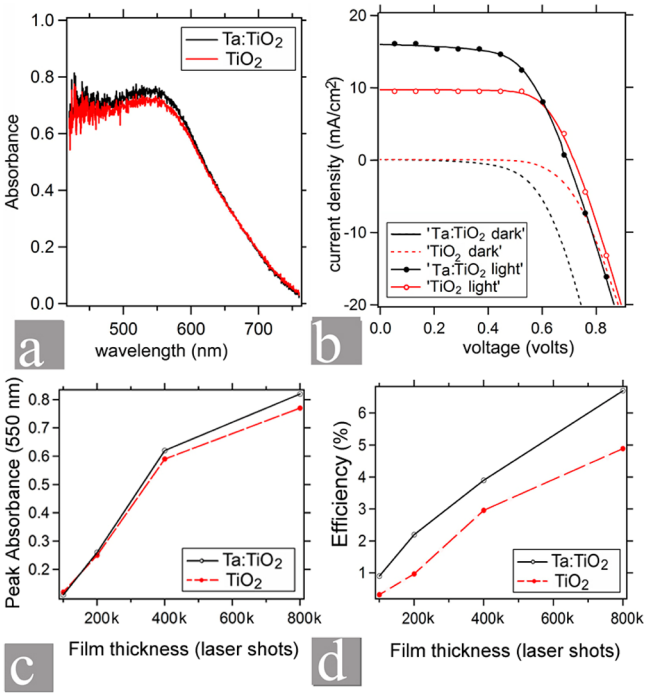

Figure 2. Top panel shows comparative studies of (a) absorbance and (b) voltage–current density plots for TiO_2 and Ta:TiO_2, the bottom panel shows (c) absorbance and (d) efficiency comparisons between TiO_2 and Ta:TiO_2 for different film thicknesses.

for Ta:TiO_2 over TiO_2 was consistent for all film thicknesses tested. The significantly higher J_{sc} combined with a nominal decrease in V_{oc} (<50 mV) upon doping with tantalum leads to a much improved overall efficiency (E_{ff}) for the Ta:TiO_2 devices (6.69%) as compared to undoped TiO_2 devices (4.9%). These trends are similar over a range of thicknesses as shown in Figure 2d and Table 1.

To rationalize the basis for the improved device performance of Ta:TiO_2 over TiO_2 it is important to evaluate the device components and processes in a stepwise manner. The first step in the operation of the DSSC is light absorption by the chromophore. Since dye adsorption on the films is comparable (Figure 2a and 2c) regardless of tantalum doping, it can be concluded that difference in light absorption by the dye is not contributing to the difference in device behavior.

Once the dye absorbs a photon, the second step in the process is injection of electrons from the excited chromophore into the conduction band of the metal oxide electrodes. The driving force for electron injection is the energy difference between the excited state reduction potential for the chromophore ($E_{1/2}(Ru^{III/II*})$) and the conduction band (CB) edge of the metal oxide. No noticeable shifts in the CB of our Ta:TiO_2 samples over undoped TiO_2 is observed from the analysis of the capacitance of the space charge layer (C_{cs}^{-2}) versus applied potential in Mott–Schottky plots (Figure 1f); however, the difference in the slopes, which are inversely proportional to the number of donors (ref 22), does point to a higher number of carriers for the Ta:TiO_2 samples.

Once injected, the electrons in the conduction band can either travel through the porous network of nanoparticles to the FTO electrode recombine with the electrolyte. Insight into both of these processes can be obtained by using electrochemical impedance spectroscopy (EIS). The results of these measurements can be seen in the Nyquist (Figure 3a) and Bode plots (Figure 3b). In the Nyquist plot, the diameter of the central arcs for Ta:TiO_2 and TiO_2 are comparable, indicating similar resistances for both porous networks. However the frequency of the peak maxima for these arcs, which is more clearly depicted in the Bode plot (Figure 3b), are dissimilar. According to Adachi et al.[23] the frequency at the maxima corresponds to the effective rate constant (k_{eff}) at which diffusing electrons are lost due to recombination. The lower k_{eff} noted for our Ta:TiO_2 samples (3.7 s^{-1}) compared to undoped TiO_2 (19 s^{-1}) points to a slower recombination rate which in turn means a lesser number of electrons lost to the back-electron transfer.

Support for the difference in recombination rates is obtained from open circuit voltage decay measurement (OCVD). The open circuit voltage is a measurement of the quasi-Fermi level which is dictated by the density of electrons in the conduction band. In the OCVD measurement, the change in V_{oc} is monitored in the dark, after a period of illumination. In this dark state there is a loss of photoelectrons and reduction in the V_{oc} due to electron recombination processes. The slower OCVD for Ta:TiO_2 compared to TiO_2 supports the conclusions from EIS (Figure 3c).

There are several trends in DSSC performance emanating from the thickness of the metal oxide films (Table 1). As expected, J_{sc} and efficiency for both TiO_2 and Ta:TiO_2 films increase with film thickness due to increased absorbance and the corresponding increase in the number of injected electrons. From table 1 we further note that the dye loading and therefore the absorbance are very similar for TiO_2 and Ta:TiO_2 for all thicknesses. The short circuit current (J_{sc}) per unit mole of dye loaded can be used as a measure of charge collection efficiencies.[13] Over all thicknesses we see a lower J_{sc} per dye loading for TiO_2 compared to Ta: TiO_2. This further points to a better charge transfer pathway for the Ta:TiO_2 than TiO_2. It is also interesting to note that for TiO_2 there is a monotonic

Table 1. Comparisons of Film Thicknesses and Device Performance for Films at Different Number of Laser Pulses for TiO_2 and Ta:TiO_2

	TiO_2				Ta:TiO_2			
laser shots	800k	400k	200k	100k	800k	400k	200k	100k
film thickness (μm)	13.5	6.7	3.4	1.7	13.4	6.8	3.4	1.7
V_{oc} (mV)	720	720	710	680	690	670	690	710
J_{sc} (mA/cm^2)	9.6	6	1.9	0.7	15.9	10.4	5.1	1.7
fill-factor	0.7	0.68	0.7	0.61	0.61	0.57	0.64	0.58
efficiency (%)	4.8	2.9	0.96	0.32	6.7	3.9	2.2	0.7
dye loaded ($\times 10^{-7}$ mol/cm^2)	0.55	0.42	0.18	0.09	0.58	0.44	0.18	0.07
J_{sc}/ dye loading (mA/10^{-7} mol)	17.45	14.28	10.55	7.77	27.41	23.63	28.33	24.28

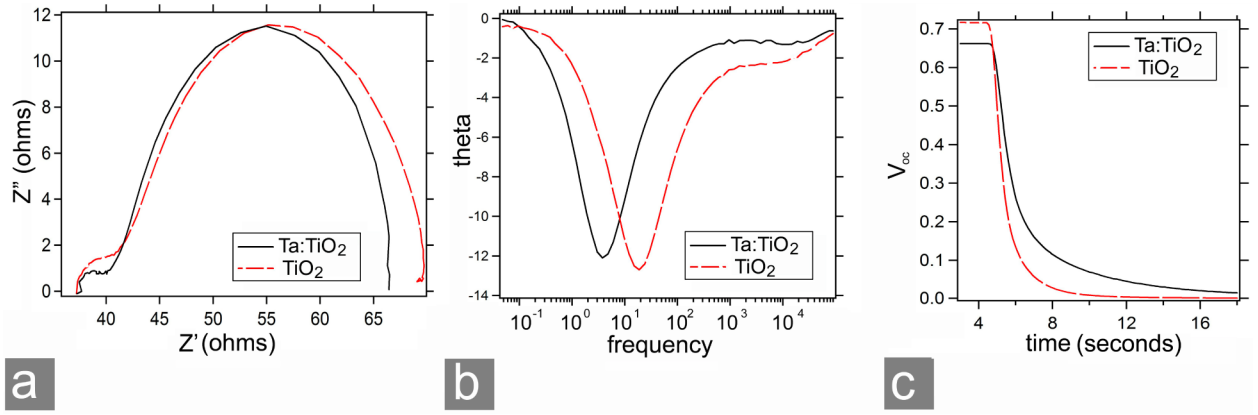

Figure 3. Electrochemical impedance spectroscopy results (a,b) and open circuit voltage decay response for TiO_2 and Ta:TiO_2 films of thickness around 13.4 μm.

improvement of this factor with increase in thickness (7.7−17.5), while for Ta:TiO_2 it is more uniform (26 ± 3) over all thicknesses as well as much higher than that of TiO_2. This points to better charge transfer for thicker TiO_2 films while the pathways for Ta:TiO_2 are much improved even at much lesser thicknesses.

Considering that carrier gradients responsible for the J_{sc} can only be built with strong light absorption and suitable diffusion and recombination characteristics, Ta:TiO_2 films with moderate absorptions do well because their superior transport properties. In contrast, the weaker transport properties of the undoped TiO_2 results in a poor J_{sc} until the light absorption capability becomes quite significant, shortening J_{sc} differences with the doped counterparts but never really catching up with them. The improvements in the diffusion parameters can actually be related to increased film conductivity. This argument is supported by EIS measurements as function of thickness and the corresponding Nyquist plots (figure 4). There is a larger increase in the arc diameters for undoped TiO_2 as the thickness increases compared to the Ta:TiO_2 films. The two important parameters from the Nyquist plots are R_w and R_k (resistance through the network and resistance in back electron transfer) are fitted and shown in Figure 4. Because of the increased electron concentration in Ta:TiO_2, both resistances are decreased. However, at smaller thicknesses the difference in R_w is much larger than the differences in R_k which accounts for the lesser improvement of APCE with thickness for TiO_2.

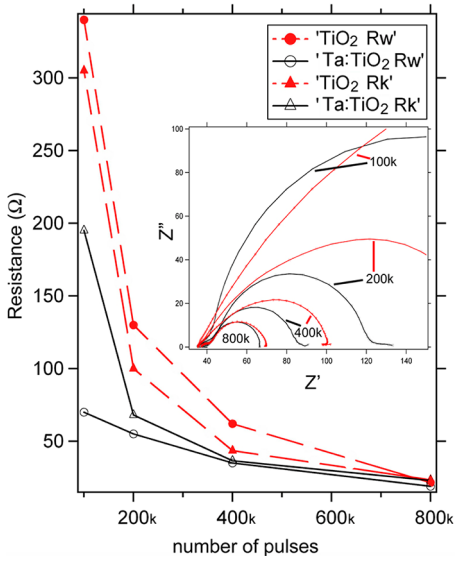

Figure 4. Changes in fitted resistances through the porous network of undoped TiO_2 and Ta:TiO_2. Inset shows Nyquist plots for different thicknesses. All thicknesses in number of laser shots used during growth.

CONCLUSIONS

To sum up, we have fabricated Ta-doped TiO_2 based DSSCs using pulsed laser deposition. The Ta:TiO_2 devices exhibit higher photocurrents without significant drop in open circuit voltage compared to those for undoped TiO_2. The increased J_{sc} values combined with a nominal decrease in V_{oc} results in over 60% improvement in overall device efficiencies for tantalum-doped films compared to undoped TiO_2. Our method of semiconductor preparation, pulsed laser deposition, completely decouples doping from other factors by producing identical morphologies for both doped and undoped films, allowing us to conclusively support that Ta doping results in a larger concentration of charge carriers, reduced recombination rate and an enhanced photocurrent.

ASSOCIATED CONTENT

Supporting Information

XRD spectra of Ta-doped and undoped TiO_2. This material is available free of charge via the Internet at http://pubs.acs.org.

AUTHOR INFORMATION

Corresponding Author

*E-mail: rln@physics.unc.edu.

Author Contributions

The manuscript was written through contributions of all authors. All authors have given approval to the final version of the manuscript.

Notes

The authors declare no competing financial interest.

ACKNOWLEDGMENTS

This material is based upon work funded by the U.S. Department of Energy, Office of Science, Office of Basic Energy Sciences under Award Number DE-SC0006416. We also acknowledge support for the use of instrumentation and help with device assembly and evaluation to the UNC EFRC

(Center for Solar Fuels, an Energy Frontier Research Center funded by the U.S. Department of Energy, Office of Science, Office of Basic Energy Sciences under Award Number DE-SC0001011) and from UNC SERC ("Solar Energy Research Center Instrumentation Facility" funded by the U.S. Department of Energy, Office of Energy Efficiency & Renewable Energy under Award Number DE-EE0003188). L.A. wishes to acknowledge financial support from research triangle solar fuels institute (RTSFI). Authors would also like to thank Chapel Hill Analytical and Nanofabrication Laboratory (CHANL) and Myoung-Ryul Ok for all their assistance.

REFERENCES

(1) O'Regan, B.; Grätzel, M. *Nature* **1991**, *353*, 3103−3109.
(2) Haque, S. A.; Tachibana, Y.; Klug, D. R.; Durrant, J. R. *J. Phys. Chem. B* **1998**, *11* (97), 1745−1749.
(3) Zhu, K.; Neale, N. R.; Miedaner, A.; Frank, A. J. *Nano Lett.* **2007**, *7* (1), 69−74.
(4) Prakasam, H. E.; Shankar, K.; Paulose, M.; Varghese, O. K.; Grimes, C. A. *J. Phys. Chem. C* **2007**, *111*, 7235−7241.
(5) Jennings, J. R.; Ghicov, A.; Peter, L. M.; Schmuki, P.; Walker, A. B. *J. Am. Chem. Soc.* **2008**, *130* (40), 13364−13372.
(6) Feng, X.; Shankar, K.; Varghese, O. K.; Paulose, M.; Latempa, T. J.; Grimes, C. A. *Nano Lett.* **2008**, *8* (11), 3781−3786.
(7) Varghese, O. K.; Paulose, M.; Grimes, C. A. *Nat. Nanotechnol.* **2009**, *4* (9), 592−597.
(8) Zhang, Q.; Dandeneau, C. S.; Zhou, X.; Cao, G. *Adv. Mater.* **2009**, *21* (41), 4087−4108.
(9) Qian, J.; Liu, P.; Xiao, Y.; Jiang, Y.; Cao, Y.; Ai, X.; Yang, H. *Adv. Mater.* **2009**, *21* (36), 3663−3667.
(10) Yong, M. J. Q.; Wong, A. S. W.; G.W. Ho, G. W. *Mater. Chem. Phys.* **2009**, *116*, 563−568.
(11) Agarwala, S.; Kevin, M.; Wong, A. S. W.; Peh, C. K.N.; Thavasi, V.; Ho, G. W. *ACS Appl. Mater. Interfaces* **2010**, *2* (7), 1844−1850.
(12) Sauvage, F.; Di Fonzo, F.; Li Bassi, A; Casari, C. S.; Russo, V.; Divitini, G.; Ducati, C.; Bottani, C. E.; Compte, P.; Gratzel, M. *Nano Lett.* **2010**, *10* (7), 2562−7.
(13) Noh, J. H.; Park, J. H.; Han, H. S.; Kim, D. H.; Han, B. S.; Lee, S.; Kim, J. Y.; Jung, H. S.; Hong, K. S. *J. Phys. Chem. C* **2012**, *116* (14), 8102−8110.
(14) Ghosh, R.; Brennaman, M. K.; Uher, T.; Ok, M. R.; Samulski, E. T.; McNeil, L. E.; Meyer, T. J.; Lopez, R. *ACS Appl. Mater. Interfaces* **2011**, *3* (10), 3929−35.
(15) Lü, X.; Mou, X.; Wu, J.; Zhang, D.; Zhang, L.; Huang, F.; Xu, F.; Huang, S. *Adv. Funct. Mater.* **2010**, *20* (3), 509−515.
(16) Chandiran, A. K.; Casas-cabanas, M.; Comte, P.; Zakeeruddin, S. M.; Graetzel, M. *J. Phys. Chem. C.* **2010**, *114*, 15849−15856.
(17) Zhang, X.; Liu, F.; Huang, Q.-L.; Zhou, G.; Wang, Z.-S. *J. Phys. Chem. C.* **2011**, *115*, 12665−12671.
(18) Feng, X.; Shankar, K.; Paulose, M.; Grimes, C. A. *Angew. Chem., Int. Ed.* **2009**, *48* (43), 8095−8.
(19) Liu, J.; Yang, H.; Tan, W.; Zhou, X.; Lin, Y. *Electrochim. Acta* **2010**, *56* (1), 396−400.
(20) Wang, Z. *Coord. Chem. Rev.* **2004**, *248* (13−14), 1381−1389.
(21) Cameron, P. J.; Peter, L. M. *J. Phys. Chem. B* **2003**, *107*, 14394−14400.
(22) Kaneko, M.; Ueno, H.; Nemoto, J. B. *J. Nanotechnol.* **2011**, *2*, 127−134.
(23) Adachi, M.; Sakamoto, M.; Jiu, J.; Ogata, Y.; Isoda, S. *J. Phys. Chem. B.* **2006**, *110* (28), 13872−13880.